Marine heatwaves and global warming impacts on winter waters in the Southern Indian Ocean

Clara Azarian, Laurent Bopp, Jean-Baptiste Sallée, Sebastiaan Swart, Christophe Guinet, Francesco d'Ovidio

Marine heatwaves and global warming impacts on winter waters in the Southern Indian Ocean

Clara Azarian 1 2, Laurent Bopp 3 , Jean-Baptiste Sallée 1, Sebastiaan Swart 4, Christophe Guinet 5 and Francesco d'Ovidio 1

1 Sorbonne Université, CNRS, IRD, MNHN, Laboratoire d'Océanographie et du Climat: Expérimentations et Approches Numériques (LOCEAN-IPSL), Paris, France.

2 Ecole Nationale des Ponts et Chaussées (ENPC), Champs-sur-Marne, France.

3 Ecole Normale Supérieure / Université PSL, CNRS, Ecole Polytechnique, Sorbonne Université, Paris, Laboratoire de Météorologie Dynamique (LMD-IPSL) Paris, France.

4 University of Gothenburg, Gothenburg, Sweden

5 Centre d'Etudes Biologiques de Chizé, UMR7372 CNRS-La Rochelle Université, Villiers en Bois, France

Corresponding author: C. Azarian; clara.azarian@locean.ipsl.fr

Abstract

In the Southern Ocean, the term “winter waters” (WWs) refers to a water mass characterized by a subsurface layer of minimum temperature that plays an important ecological role for marine ecosystems, and in particular for top predators. Given that the Southern Ocean is experiencing warming and intense marine heatwaves (MHWs), particularly at subantarctic latitudes, we investigate here how different levels of warming might impact the presence, depth and minimum temperature of WWs in the Indian sector of the Southern Ocean. In particular, we assess how WWs are impacted by surface MHWs using *in situ* Argo hydrographic observations and biologging data. The results indicate that WWs are substantially reduced, deeper and warmer during the presence of MHWs. Using the most recent climate projections, we find a significant, but scenario-dependent, southward shift of WWs under global warming. Potential impacts of such WW shifts on pelagic ecosystems, at different timescales (from daily to decadal), are discussed.

Keywords: Southern Indian Ocean ; winter waters ; marine heatwaves ; global warming

1. Introduction

"Winter waters" (WWs) is a term used to qualify the subsurface minimum temperature layer present in the Southern Ocean. The Polar Front, one of the most prominent hydrographic features in this basin, is often defined as its northernmost extension (Gordon and Huber, 1984; Park et al., 1998; Pauthenet et al., 2018). WWs are formed from the freezing cold surface waters of the winter mixed layer of the subpolar Southern Ocean, and are then capped by a warmer and fresher surface layer in spring-summer as sea-ice melts and air temperature warms. This seasonal cycle leaves behind a cold water mass in the subsurface between about 100 and 400 m, which is stably stratified by the vertical salinity profile (Sharma and Matthew, 1985; Park et al., 1993; Belkin and Gordon, 1996). WWs temperature typically ranges between -2°C and 3°C (Gordon, 1975 ; Park et al., 1993 ; Sabu et al., 2020).

The distributions and characteristics of WWs depend on large-scale drivers such as wind stress or sea-ice extent (Gordon and Huber, 1984), which are expected to change under global warming (Lee et al., 2021). Water masses of the Southern Ocean are overall observed and projected to continue to warm in the future (Sallée et al., 2013; Sallée et al., 2018; Auger et al., 2021). The observed temperature change across the Southern Ocean is actually heterogenous. Cooling is observed in the southern end of the Southern Ocean, while warming occurs at depth and also within and north of the Antarctic Circumpolar Current (ACC; Armour et al., 2016; Llovel et al., 2016; Morrison et al., 2016; Sallée et al., 2018; Auger et al., 2021; Fox-Kemper et al., 2021). No warming trends have yet been reported for the WWs and their future evolution remains uncertain.

In this paper, we aim at shedding light on the impact of a warming climate on WWs. As WWs are characterized by a minimum of temperature, their distribution and characteristics can be expected to be affected by a warming climate. Our main motivation in this endeavor is underpinned by the demonstrated importance of this water mass for Southern Ocean ecosystems. WWs have been shown to play a structuring role for pelagic ecosystems and for the vertical distribution and relative abundance of mesopelagic organisms (Béhagle et al., 2017; McMahon et al., 2019; Hunt et al., 2021). WWs in particular are associated with mesopelagic organisms being more concentrated towards the surface and thus easily accessible prey for top predators (e.g. king penguins, *Aptenodytes patagonicus*, Kooyman et al., 1982; Kooyman et al., 1992).

There are two main ways climate change could impact WWs characteristics. First, changes in large-scale circulation patterns may alter the distribution of WWs, and in particular the southward shift of the Polar Front or the increase of eddy shedding southward from the Polar Front may push WWs southward and change their distribution. Second, local surface warming occurring at the time of WWs formation in winter, or penetrating downward in spring-summer by diffusion or vertical mixing, could warm WWs, or eventually erode the temperature minimum entirely. Here, we first use observation-based datasets to test the hypothesis that anomalously warm surface conditions affect WWs distribution and characteristics through one or a combination of these two processes. Second, we use climate models to investigate how these processes unfold into a net change in WWs distribution and characteristics under a diverse range of global warming levels.

Anomalously warm surface conditions are commonly referred to as marine heatwaves (MHWs; Hobday et al., 2016; Frölicher et al., 2018; Oliver et al., 2021). There is increasing evidence that MHWs detected at the surface can penetrate to depth (Elzahaby and Schaeffer, 2019; Darmaraki et al., 2019; Hu et al., 2021; Miyama et al., 2021; Großelindemann et al., 2022), with the potential to locally modify subsurface water masses characteristics such as WWs. In addition, it was shown that MHWs in the southern Indian basin can be associated with a southward shift of the Polar Front, which in 1997 led to a mass mortality of Crozet king penguins as their foraging zones were shifted too far south from their breeding island (Bost et al., 2015). We see here the importance of better understanding the impact of warm surface conditions on WWs, which can have dramatic consequences for ecosystems. Such extreme events can be seen as a snapshot into the future under a warmer climate. However, dominant processes at short and long timescale can differ, so that a proper analysis of future projections must also be carried out before any conclusions are drawn.

We focus our study on the Indian sector of the Southern Ocean because this is one of the regions of the world that has experienced the largest increase in ocean heat content in recent decades (Roemmich et al., 2015; Llovel et al., 2016; Sallée et al., 2018; Fox-Kemper et al., 2021). It has also been shown that the position of the Polar Front can be highly variable west of the Kerguelen Plateau (Pauthenet et al., 2018). Since this region also hosts a rich biodiversity and notably top predators whose behavior and foraging success has been related to physical properties of water masses (McIntyre et al., 2011; Guinet et al., 2014), the Southern Indian Ocean is of particular interest to study how warming can impact WWs and, in turn, pelagic ecosystems.

The paper is organized as follows. First, we investigate the relationship between WWs and surface extreme temperature anomalies, combining *in situ* data with multisatellite observations and a 1/12° ocean reanalysis product. This is motivated by the findings that the pattern of intense MHWs at the northern boundary of the ACC might be associated with mesoscale eddies (Su et al., 2021) and that, consequently, advective processes could shift the position of WWs locally. This first part shows that both advective and local diffusion processes related to surface warming can contribute to reducing WWs extent or signal. We also highlight potential biases in the MHWs characteristics sampled by elephant seals compared to random sampling by Argo floats. Second, we investigate how these impacts on WWs are intensified under global warming, leading to a reduced extent of WWs, using CMIP6 models. Finally, we discuss the potential mechanisms driving MHWs and global warming impacts on WWs distribution, the contrast between observed trends, projections and paleoceanographic studies and the potential ecological implications of a southward shift of the WWs.

2. Material and Methods

2.1. Observations and Mercator reanalysis

Temperature *in situ* profiles are collected from Argo float data between 2001 and 2019 over the area 20 -120°E 70-30°S (Argo, 2000). We download 170 352 profiles, among which 78 407 are complete between 5 and 900 m. Temperature *in situ* profiles are also collected between 2004 and 2017 from biologging in the Southern Indian Ocean and gathered by the Marine Mammals Exploring the Oceans Pole to Pole or MEOP consortium (Treasure et al., 2017; Roquet et al., 2014). We download 140 436 profiles, among which 9 484 are complete between 5 and 900 m.

The GLORYS12V1 product is the Copernicus Marine Environment Monitoring Service (CMEMS) global ocean eddy-resolving reanalysis delivered by Mercator Ocean. This product provides daily and monthly mean temperature over 50 vertical levels and with 1/12° horizontal resolution between 1993 and 2019. This product is used in this paper to provide a monthly climatology for the vertical temperature profiles. The GLORYS12V1 product is also used to determine the probability of presence of WWs between 1993 and 2019. This probability is estimated by detecting, for each day between 1993 and 2019 and for each grid cell, whether the minimum temperature between 100 and 400 m is found at a depth less than 350 m, and then averaging the results (0 for absence of a temperature minimum in this interval, 1 for presence) over time. WWs are also characterized by the temperature at the minimum (also named WWs temperature) and the depth of this minimum (also named WWs depth), as in Sabu et al. (2020).

The Operational Sea Surface Temperature and Ice Analysis (OSTIA) system run by the UK's Met Office (Good et al., 2020) provides daily sea surface temperature free of diurnal variability, also called the foundation sea surface temperature, at a 0.05° x 0.05° horizontal grid resolution between 1982 and 2019. This product combines satellite measurements (L4 level) from both infrared and microwave radiometers with in-situ measures from ships, drifting and moored buoys. This dataset was used for surface MHW detection.

2.2. Marine heatwaves detection and characteristics

A MHW is identified as an event of at least 5 days for which the sea surface temperature (SST) is above the 90th percentile of a data distribution using a seasonally-varying climatology for each grid point and for each day of the year using an 11-day window (Hobday et al., 2016). The threshold is also smoothed by applying a 30-day moving average. An average of 24 days/year under MHW is estimated between 1993 and 2019 over the area 20-120°E, 58-40°S.

The temperature anomaly depth, also called “MHW depth” in Elzahaby and Schaeffer (2019), is calculated to investigate whether surface MHWs are associated with deeper temperature anomalies (see Supplementary Methods). To do so, temperature anomaly profiles are obtained using the combination of information from different datasets:

- OSTIA dataset: for the detection of surface MHW using Hobday et al. (2016) definition (90th percentile)
- Argo float data: daily hydrographic profiles
- MERCATOR reanalysis: provide for each grid cell a monthly climatology profile

From each Argo hydrographic profile, we compute the vertical cumulative temperature anomaly, and the depth where 95% of the cumulative temperature anomaly is reached, also named “temperature anomaly depth”. Temperature anomalies are defined as a departure from a seasonal climatological mean produced from an ocean reanalysis (MERCATOR). Using satellite SST, we then group each of these profiles as within a MHW or outside. The Argo profile is said to be in a MHW according to the surface detection of a MHW using sea surface temperature observations (OSTIA). A bootstrap approach with 10000 iterations is used to obtain the mean values of the two metrics, as the sample sizes (in and out MHW) differ.

2.3. Altimetry analysis

Altimetry-derived geostrophic velocities are computed by CLS/AVISO (Collecte Localization Satellites/Archiving, Validation, and Interpretation of Satellite Oceanographic data) and distributed by Copernicus Marine Environment Monitoring Service (CMEMS) as a gridded product on a 0.25° x 0.25° horizontal grid resolution between 1993 and 2020 (https://doi.org/10.48670/moi-00148).

Using AVISO geostrophic velocities, the latitudinal advection of water parcels over 15 days backward in time is estimated. The latitudinal displacement is positive when the water parcel has moved

8

180 southward over the last 15 days. The duration of 15 days for the advection is chosen as this is the typical
181 timescale for MHW durations (Oliver et al., 2018). A monthly climatology of latitudinal displacement is
182 determined over multiple years (1993-2020). Correlations between anomalies of latitudinal
183 displacement and the presence/absence of MHW are evaluated to investigate the co-occurrence between
184 MHW and an anomalous southward displacement of surface warmer water.

185

186 ## 2.4. CMIP6 models

187

188 Coupled models from the Coupled Model Intercomparison Project 6 (CMIP6) have been used to
189 conduct historical and projection simulations notably to investigate how the Earth system responds to
190 forcing (Eyring et al., 2016). The 12 models used here (described in Supplementary Material S1) are
191 selected among 26 CMIP6 models as they provide a realistic representation of the circumpolar mean
192 position of WWs between 1995-2014 using their historical simulations (Supplementary Methods and
193 Supplementary Material S2). Historical (1850-2014) and projection (2015-2100) simulations from
194 CMIP6 are used here. Three emission trajectories, also called Shared Socioeconomic Pathways (SSPs),
195 are considered: the SSPs 1-2.6, 2-4.5 and 5-8.5 (Lee et al., 2021). The variable considered here is
196 monthly *thetao* (sea water potential temperature across different depth levels in °C). WWs are detected
197 through the presence of a temperature minimum between 100 and 400 m at a depth less than 350 m. The
198 outputs of the 12 models under the three SSPs are combined following the so-called 'time-shift
199 approach', which consists in averaging the models outputs over a period that, for each model,
200 corresponds to a given global warming level (GWL ; Herger et al., 2015; Chen et al., 2021; Lee et al.,
201 2021; see Supplementary Methods).

202

9

3. RESULTS

3.1. Winter waters distribution and modulation by marine heatwaves

Based on the MERCATOR reanalysis product presented above, we describe the typical characteristics of WWs in the Southern Indian Ocean (20-120°E, 70-30°S). On average between 1993-2019, their northernmost extension is estimated to be between 52°S and 46°S, and it can be noted that at their northern edge, WWs presence is no longer continuous as illustrated on Figure 1A. WWs mean temperature is 1.3°C but varies between -0.55°C and 3°C depending on the latitude/longitude (Figure 1D ; note that we use a maximum historical WWs temperature at 3°C; see Supplementary Methods) and WWs mean depth is 155 m and varies between 110 and 280 m (Figure 1 C). By definition, the water mass north of the WWs is not characterized by a minimum temperature between 100 and 400 m and is warmer than the water masses south of the Polar Front throughout the upper 400 m (e.g. Figure 1A). We now focus on the variability of presence, temperature, and depth of WWs and seek to determine what is the influence on its variability of warm surface events, such as marine heatwaves.

10

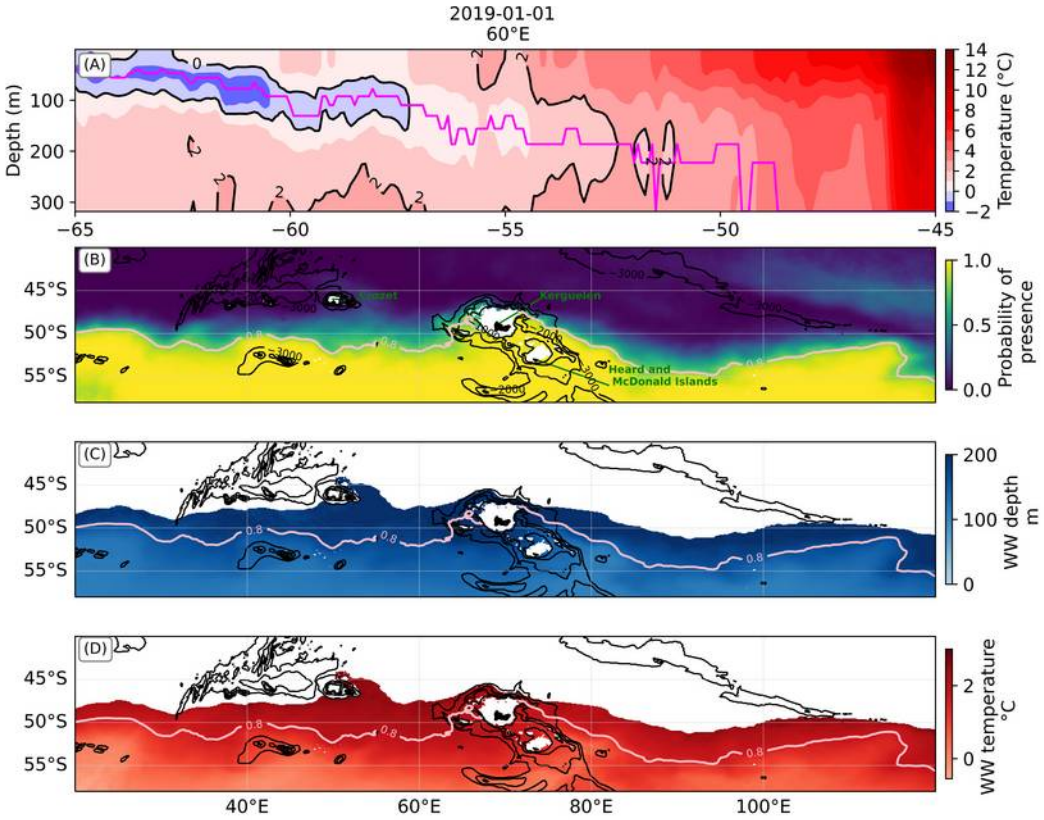

Figure 1: Winter waters climatological description and characteristics using MERCATOR reanalysis product between 1993 and 2019. (A) Example of the vertical signature of winter waters (minimum temperature between 100 and 400 m) at 60°E on the 1st of January 2019. The position of the minimum temperature along the cross section is indicated in magenta. The characteristics of the winter waters studied here are the probability of presence of winter water (B, presence is 1, absence is 0), the depth of the minimum temperature (C) and the temperature minimum value (D). A mask to only select grid cells where on average the minimum temperature is below 3°C was used on C and D. The contour of the 80% probability of presence of winter waters is shown in pink on B, C and D.

11

3.1.1. Southward shift of winter waters distribution under marine heatwaves

We first seek to determine whether MHWs are deep reaching in the Indian sector of the Southern Ocean. In MHWs, the temperature anomaly depth is 3 times deeper than outside MHWs (Figure 2B), highlighting that MHWs are not limited to the surface layer but extend at depth. We note that outside MHWs the mean temperature anomaly depth is by construction much shallower because many profiles associated with null or negative vertical temperature anomalies would be associated with a depth of 0. Consistent with the estimated difference in temperature anomaly depth, in MHWs, the typical cumulative temperature anomaly is much larger than outside, almost 5 times larger, with a mean cumulative temperature anomaly estimated at 549 °C.m (± 8 °C.m; Figure 2C).

12

Figure 2: (A) Spatial distribution of 78407 Argo hydrographic profiles that are complete up to 900 m between 2001 and 2019. Mean MHW depth (B) and mean cumulative temperature anomaly (C) calculated from the anomaly profiles between Argo profiles and a monthly reference obtained with MERCATOR reanalysis over the area 20-120°E, 70-30°S. The mean values of the two metrics, in and out of a MHW, are shown (dashed vertical lines). Examples of Argo profiles in a MHW (red; 30.1°E/53.2°S on 20/11/2019 (D); 37°E/51.8°S on 10/12/2015 (E)) and outside a MHW (blue; 30.1°E/54°S on 20/11/2013 (D); 37.9°E/52°S on 08/12/2014 (E);) together with associated monthly reference from MERCATOR reanalysis (black solid for reference to Argo observation out a MHW; black dashed for reference to Argo observation in a MHW). The temperature anomaly depths associated with these profiles are shown directly on (D) and (E) and reported on (B) for the MHW cases (dotted lines).

As MHWs are associated with deeper and intense temperature anomalies (Figure 2), we investigate whether this is due to a replacement of water masses through the southward advection of warmer waters. Positive correlations are found across the Indian sector of the Southern Ocean between an anomalous southward latitudinal displacement of water parcels over 15 days (typical MHW duration ; the convention used here is that the latitudinal displacement is positive when the water parcel has moved southward), and the presence of MHW, estimated using OSTIA dataset, between 1993 and 2020 (mean correlation coefficient over the area of 0.2, Figure 3A). These correlations are higher in the area where the most intense MHWs have previously been found (see Figure 3A in Azarian et al., 2023), north of the Southern ACC Front between 20°E and 40°E and between the Subantarctic Front and the Northern boundary between 40°E and 70°E (correlation coefficient of more than 0.3 and up to 0.87 ; Figure 3A). MHWs are therefore associated with the southward advection of water. If this occurs across the Polar Front, within mesoscale eddies or front meanders, it would imply that northern and warmer water mass es are advected southward, effectively pushing WWs southward, and generating a deep positive temperature anomaly (e.g. Figure 2B). Indeed, the water mass north of the northernmost extension of WWs often have transitional properties between Antarctic Surface Waters and Subantarctic Surface Waters (the latter dominates north of the Subantarctic Front), with temperatures typically ranging

between 3° and 8°C, though their properties mostly depend on mixing (Carter et al., 2008). Consistently, we find that the presence of MHW significantly decreases the probability of presence of WWs, using MERCATOR ocean reanalysis between 1993 and 2019 (Figure 4A). This southward shift of WWs in presence of MHWs is also consistent with *in situ* observations analysis (Supplementary Materials S3).

The impact of warm ocean surface conditions on WWs can therefore come from a southward water transport that would cause both a local MHW and a displacement of WWs further southward. This is illustrated by the example on Figure 2E: there is no longer a minimum temperature on the Argo profile during the MHW and the profile is warmer than the MERCATOR reference at the same location throughout the water column, suggesting the presence of a different water mass. However, remaining WWs temperature and depth can also be directly affected: either because their distribution is shifted or because of vertical heat diffusion. This is illustrated by the example on Figure 2D: the temperature anomaly during the MHW is the most intense at the surface and there is still a minimum temperature, although this minimum is deeper and slightly warmer than the MERCATOR reference at the same location. Indeed, WWs in MHWs are deeper and warmer than WWs that are not in a MHW (Figure 4 B and C). The mean difference between the mean WWs depth anomaly in and out MHWs is around 17 m (± 25 m, spatial standard deviation). The mean difference between the mean WWs temperature anomaly in and out MHW is around 0.33°C (±0.45°C, spatial standard deviation).

We note that the spatial patterns of warming and deepening during MHWs tend to follow mean dynamic topography contours, which represent the general circulation (Figure 4). In particular, changes are weaker in areas of northward cold water mass intrusion such as around Conrad Rise (20-26°E), the Fawn Trough (74-83°E) or east of the Southeast Indian ridge (110-116°E). Hotspots of deepening and warming of WWs under MHWs are found west of Crozet Plateau (25-34°E) and east of Kerguelen Plateau (76-102°E), which are standing meanders and areas of high eddy kinetic energy (Figure 4 ; Siegelman et al., 2019; Dove et al., 2022). The differences between WWs temperature anomalies (and depth anomalies) in MHWs compared to outside MHWs are two to three times warmer (and deeper) in these two locations compared to the regional mean of those differences. These two locations also

correspond to the areas where the difference between the probability of presence of WWs given a MHW and the probability of presence of WWs given no MHW is the strongest. The probabilities of WWs presence given a MHW are 71% lower (than those given no MHW) on average in these two locations and up to 100% lower. A 100% decrease means that no WW is detected during a MHW in a grid cell where WW can be detected when there is no MHW.

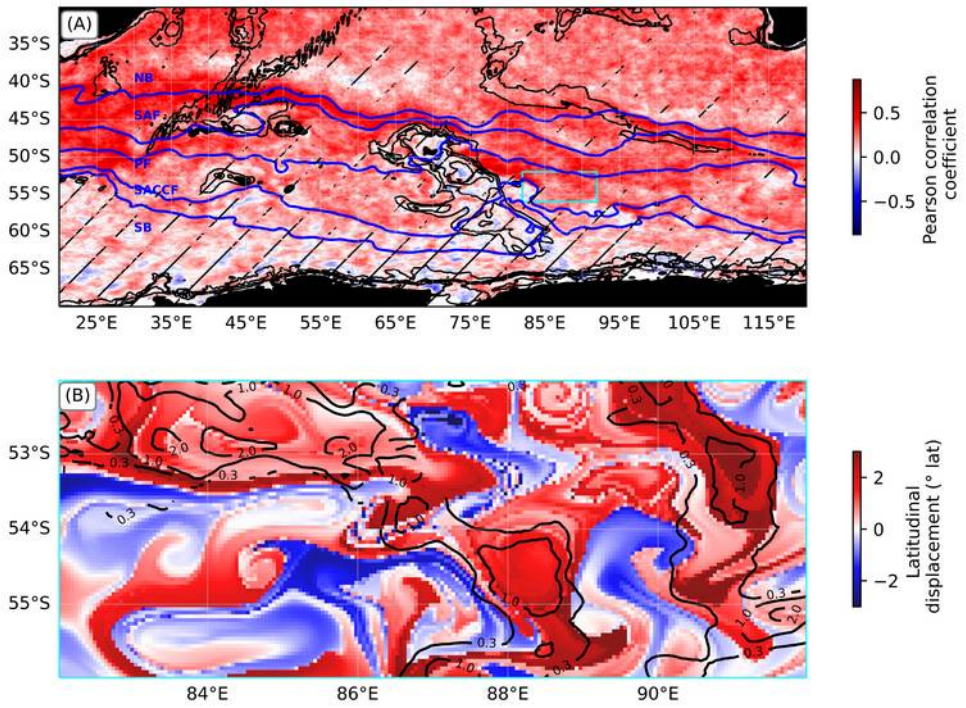

Figure 3: (A) Correlation between the latitudinal displacement anomaly (using AVISO geostrophic velocities) and the presence/absence of marine heatwaves (MHWs, using OSTIA daily data and Hobday et al., 2016 definition, 90th percentile) using monthly averages over multiple years between 1993 and 2020. The Antarctic Circumpolar Current (ACC) fronts such as the Subantarctic Front (SAF), the Polar Front (PF) and the Southern ACC front (SACCF), as well as the Northern (NB) and the Southern (SB) boundaries are shown in blue (from Park and Durand, 2019). Hatched areas indicate where the results are not significant ($p>0.01$). (B) Example of the overlap between marine heatwaves intensity and the

15

latitudinal displacement over 15 days on the 27th of december 2017 over the area 82-92°E 56-52°S (area shown in cyan in A). The black contours correspond to MHW intensity of 0.3°C, 1°C and 2°C.

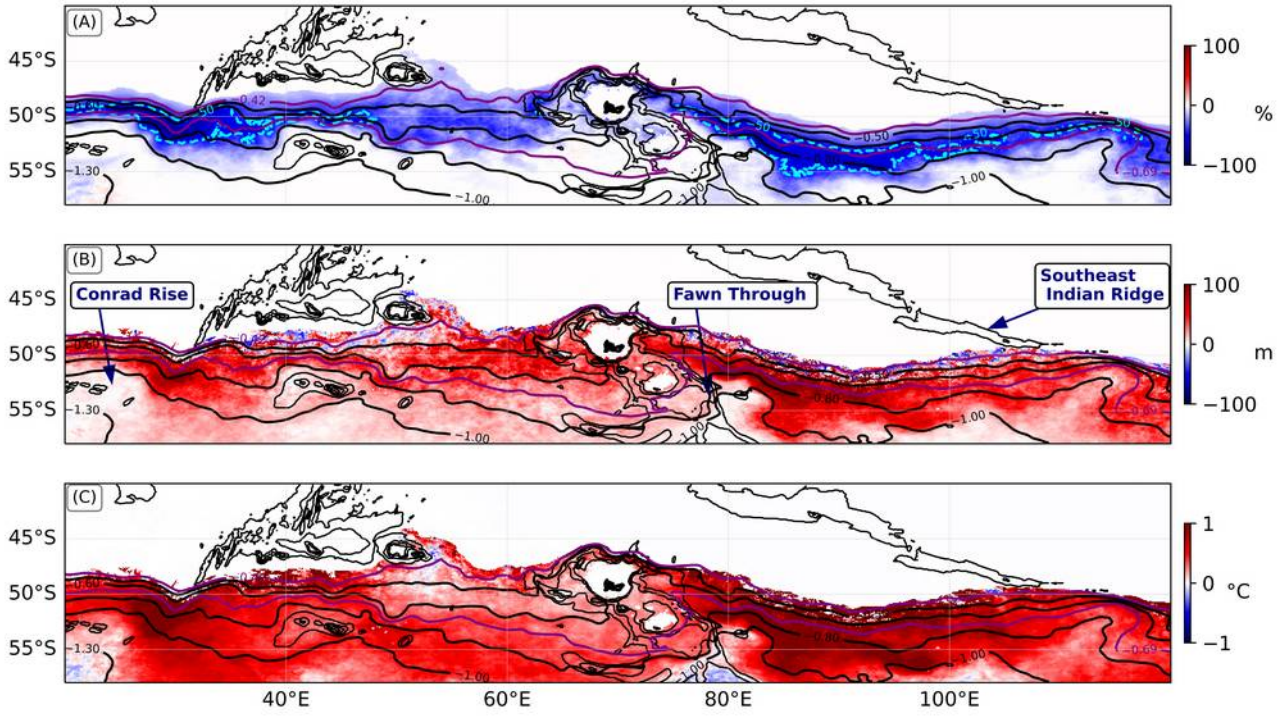

Figure 4: Impacts of marine heatwaves (MHWs) on winter waters (WWs) using MERCATOR reanalysis product between 1993 and 2019, through (A) the difference between the probability of presence of WWs given that there is a MHW and the probability of presence of WWs given that there is not a MHW (contour of 50% difference in cyan); (B) the difference between the WW depth anomaly (relative to a monthly climatology, 1993-2019) in and out of a MHW; and (C) the difference between the WWs temperature anomaly (relative to a monthly climatology, 1993-2019) in and out of a MHW. A mask to only select grid cells where a minimum temperature between 100 and 400 m less than 3°C is observed on average over 1993-2019 is applied on these figures. Mean dynamic topography contours (mean between 1993 and 2012, HYBRID-CNES-CLS18-CMEMS2020, Mulet et al., 2021) are shown in black, with the -0.69 and -0.42 m contours, which have been respectively associated with the southern and northern branches of the Polar Front (Chapman et al., 2017), that are shown in purple on these figures.

16

3.1.2. Shallow and cold bias in marine heatwaves sampled by elephant seals

Elephant seals often forage near the Polar Front and can rely on oceanographic conditions to adapt their foraging strategy (McIntyre et al., 2011; Guinet et al., 2014). MEOP-CTD dataset (see section 2.1) provides elephant seals hydrographic profiles that can be used to evaluate the temperature anomaly depth during extreme events, as previously done with Argo float data. The aim here is to identify possible biases in the water masses properties sampled by elephant seals in respect to Argo estimates.

We investigate in particular the depth of temperature anomalies during MHWs sampled by elephant seals near the Polar Front east of the Kerguelen Plateau (80-100°E; 55-45°S), which is an important foraging area (Bost et al., 2009; Dragon et al., 2010; Cotté et al., 2015; Allegue et al., 2022), and as such represents a region where both elephant seal and Argo data are available (Figure 2A and 5A). We use 467 MEOP-CTD profiles available between 2004-2017 (Figure 5A) and 4101 Argo profiles between 2001 and 2019. The mean temperature anomaly depth is 7% shallower and the mean cumulative temperature anomaly is 21% less intense using elephant seals data compared to Argo data, although those same metrics outside a MHW are similar for both datasets (Figure 5B,C). These results suggest that elephant seals do not sample (i.e., avoid) deeper and more intense marine heatwaves. While MEOP-CTD dataset is complementary to Argo data, using elephant seal data to study MHWs can therefore introduce a bias towards shallower and less intense MHWs possibly due to animal preference to avoid higher-than-normal temperatures.

17

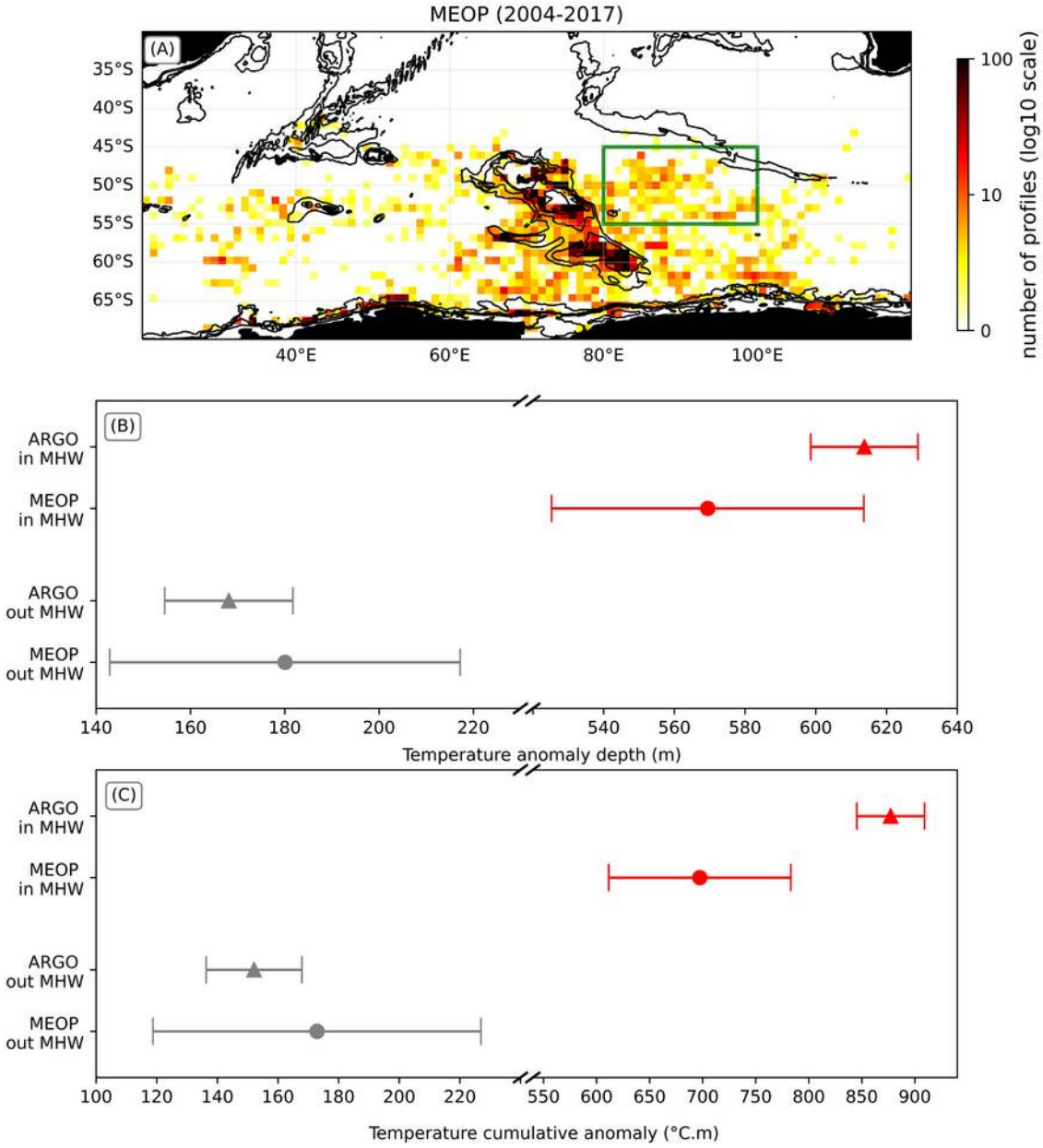

Figure 5: Spatial distribution of 9484 hydrographic profiles that are complete up to 900 m, from MEOP-CTD dataset between 2004 and 2017 (A). Mean temperature anomaly depth (in m, B) and mean cumulative temperature anomaly (°C.m, C) calculated from the anomaly profiles between elephant seals profiles (round marker) or Argo profiles (triangles) and a monthly reference obtained with MERCATOR reanalysis. These calculations are done both for profiles found in (red) and out (gray) a

18

MHW respectively over the area 80-100°E 55-45°S (green rectangle on A). The mean values and errorbars are estimated using a bootstrap approach, as presented in section 2.2.

3.2. Winter waters in the future for different warming levels

In the previous section, we show that in the past decades transient warm ocean surface events are associated with anomalies in WWs characteristics, as WWs can shift southward or be warmed and deepened, due to advective processes or local diffusion. In this section, we now seek to determine if in a globally warmer climate, WWs would be affected durably in similar ways.

Consistently with a southward water mass displacement, as global warming levels increase, the northernmost position of WWs (defined as the 80% probability of presence; referred to as Polar Front) shifts southward in CMIP6 models. The mean southward shift is 1.6° (±0.9°, along longitudes standard deviation), 2.1° (±1.3°), 3.1° (±1.4°) and 5.2° latitude (±1.5° latitude) when averaged from 20°E to 120°E, for GWL 1.5°C, 2°C, 3°C and 4.5°C respectively (Figure 6).

There is an important asymmetry in the WWs southward shift between east and west of the Kerguelen Plateau. West of the Kerguelen Plateau (20-70°E), WWs shift southward by around 2.2°, 2.8°, 3.9° and 5.9° latitude for GWLs 1.5°C, 2°C, 3°C and 4.5°C, respectively. East of the Kerguelen Plateau (70-120°E), the WWs shift southward by around 1°, 1.4°, 2.3° and 4.6° latitude for GWLs 1.5°C, 2°C, 3°C and 4.5°C, respectively (Figure 6). Compared to the western side of the plateau (65-70°E), on the eastern side of the Kerguelen Plateau (75-80°E), the Polar Front is relatively stable for low warming levels before shifting southward (Figure 7). This relative stability of the Polar Front east of the Kerguelen Plateau is however very dependent on the chosen models. For each model and each scenario, we determine the global warming level for which the Polar Front position anomaly in absolute starts to be permanently greater than 0.4° latitude (that is twice the mean natural variability of the Polar Front position between 75-80°E across models and scenarios). East of the Kerguelen Plateau, this mean threshold is 2.6 °C (±0.6°C, intermodel and inter scenarios standard deviation; Figure 7C).

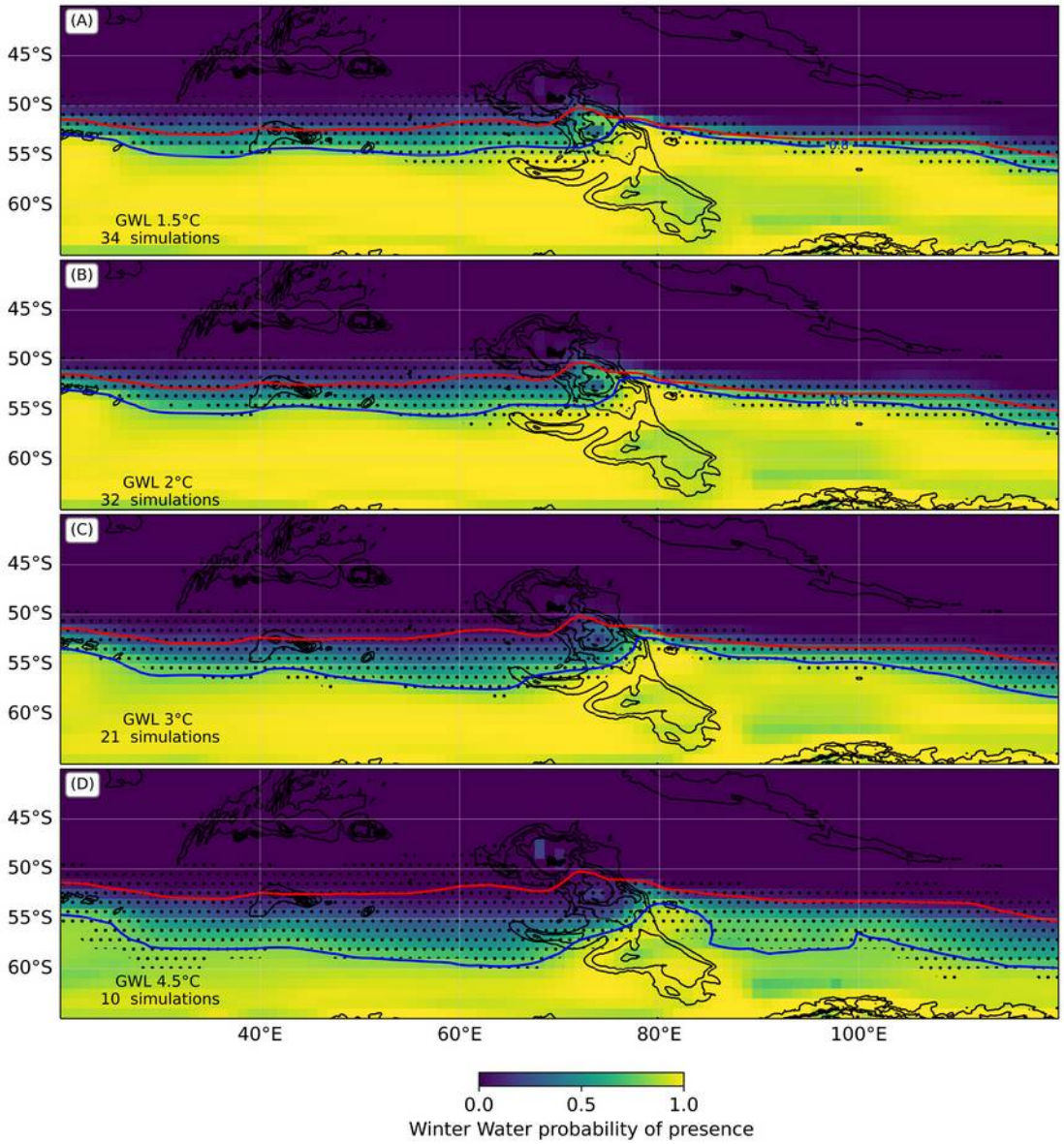

Figure 6: Winter waters probability of presence for a global warming level of 1.5°C (A), 2°C (B), 3°C (C) and 4.5°C (D) relative to 1850-1900 using 12 CMIP6 models and SSP1-2.6, SSP2-4.5 and SSP5-8.5. The blue contours indicate the northernmost limit of 80% probability of presence of winter waters for each global warming level. The red contours indicate the northernmost limit of 80% probability of presence of winter waters for the preindustrial period (1850-1900) for the same number of simulations in each case. Dotted areas indicate where at least 80% of the simulations agree with the sign of the change of presence/absence of winter waters relative to 1850-1900.

20

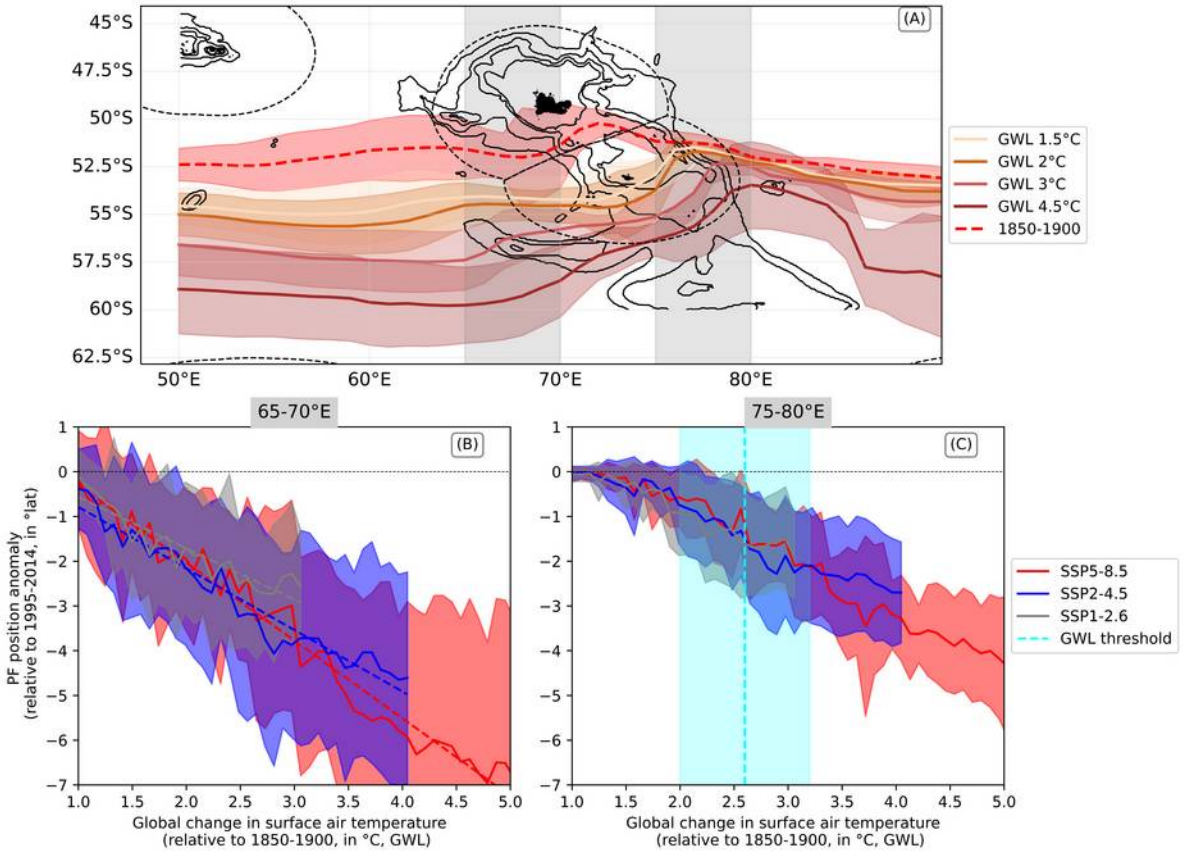

Figure 7: Northernmost limit of 80% probability of presence of winter waters (similar to Figure 6) for global warming levels (GWLs, global change in surface air temperature) 1.5°C, 2°C, 3°C and 4.5°C, as well as for the preindustrial period (1850-1900, dashed red line) between 50° and 90°E (A). The colored areas on (A) correspond to the intermodel standard deviation. Polar Front (PF) position anomaly (relative to 1995-2014) for the average of 12 CMIP6 models under SSP1-2.6 (gray), SSP2-4.5 (blue) and SSP5-8.5 (red), averaged over 65-70°E (B) and 75-80°E (C) for different GWLs (relative to 1850-1900). The two areas studied are shown in gray on panel A. The solid lines correspond to the multimodal mean value and the colored areas represent the intermodel standard deviation. On panel B, the dashed lines represent the linear regression of the PF position anomaly (over 65-70°E) with global warming for the different scenarios. On panel C, the vertical dashed line indicates the mean value, across the different models and scenarios, of the global warming threshold for which the PF position anomaly in absolute

21

starts to be permanently greater than 0.4° latitude (that is twice the natural variability of the PF position east of the Kerguelen Plateau ; referred to as GWL threshold).

We next investigate how the remaining WWs shifted southward are affected by local warming under the different global warming levels. Under all future warming levels, WWs are projected to warm (Figure 8). When averaged over the area 20-120°E, 70-30°S, the mean change of temperature (relative to 1850-1900) for the multimodel mean is 0.6°C (± 0.3°C, regional mean intermodal standard deviation), 0.8°C (± 0.4°C), 1.1°C (± 0.5°C), 1.4°C (± 0.6°C) for respectively GWLs 1.5°C, 2°C, 3°C and 4.5°C (Figure 8). Compared to the warming, the overall projected deepening of WWs under global warming is relatively weak and not significant for a large proportion of our region of interest, especially east of the Kerguelen Plateau (Supplementary Material S4). The area-average deepening ranges from 5 to 9 m between GWL 1.5°C and 4.5°C but changes in WWs depth vary widely spatially within a single model and between models (Supplementary Material S4).

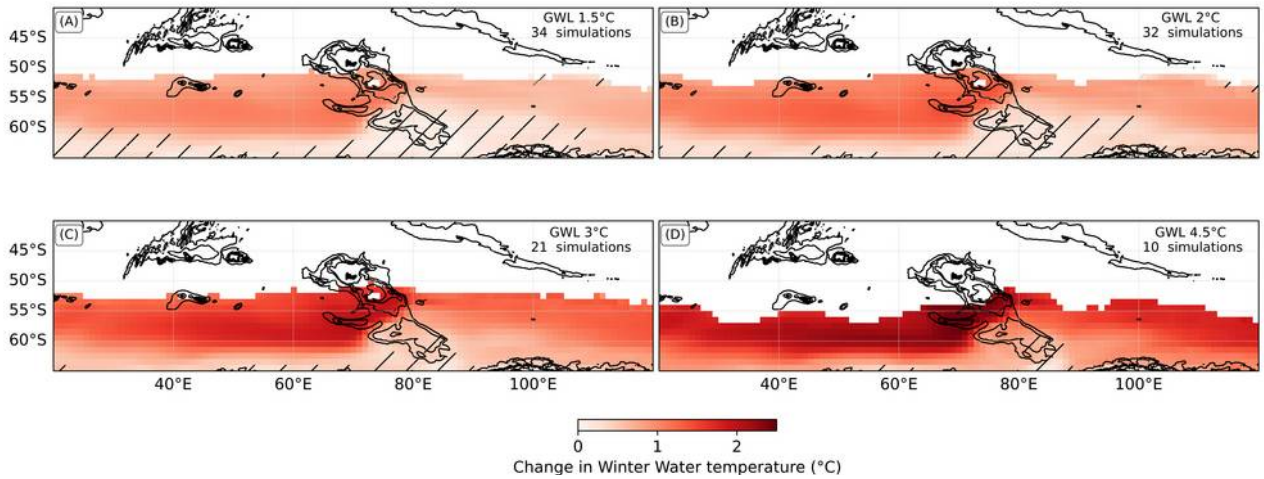

Figure 8: Change in winter waters' temperature for a global warming level of 1.5°C, 2°C, 3°C and 4.5°C relative to 1850-1900 using 12 CMIP6 models and SSP1-2.6, SSP2-4.5 and SSP5-8.5. Only mean values obtained from more than 80% of the simulations are shown (as winter waters shift differently

22

depending on models). Hatching indicates areas where the intermodel standard deviation is superior to the multimodel mean.

4. DISCUSSION

4.1. Rapid winter waters variability associated with marine heatwaves

Our study shows that MHWs can be associated either with a replacement of WWs or with warmer and deeper WWs (see section 3.1).

Our findings suggest that MHWs in the Southern Indian Ocean can be related to the regional mesoscale activity. Surface mean MHW intensity patterns show that the most intense MHWs are located along the northern boundary of the ACC (as defined in Park et al., 2019) in areas of high SST variability but also east of the Kerguelen Plateau in high eddy kinetic energy areas (Su et al., 2021; Azarian et al., 2023). Consistently, Su et al., 2021 show, using an eddy-resolving model and NOAA-OI observations, the similarity between patterns of surface temperature anomalies and of sea level variability, used as a proxy for eddy activity, east of the Kerguelen Plateau. East of the Kerguelen Plateau (80-100°E; 55-45°S), we observe that MHWs sampled by elephant seal are shallower and less intense (Figure 5). This area east of Kerguelen is a major foraging zone for elephant seals females and juveniles (*Mirounga leonina*) whose behavior is related to mesoscale activity near the Polar Front (Bailleul et al., 2010; Dragon et al., 2010; Cotté et al., 2015 ; Cox et al., 2020). Elephant seals were found to avoid the interior of anticyclonic structures for capturing prey (Dragon et al., 2010). The observed bias of subsurface MHWs characteristics with MEOP-CTD datasets compared to Argo floats data (Figure 5) is thus consistent with MHWs being strongly associated with anticyclonic eddies. Also, Argo-derived MHW presence is found consistently in locations with higher eddy kinetic energy compared with profiles outside MHWs, especially in winter (Kolmogorov-Smirnov statistic-test=0.12, p-value=2.4 $.10^{-22}$; Supplementary Material S5).

In this study, we show that MHW occurrence is positively correlated to a southward advection of water, especially at the northern boundary of the ACC (correlation coefficient up to 0.87; Figure 3). The advection of water parcels showed that MHW are associated with southward latitudinal displacements that, on timescales of the order of a MHW duration (15 days), can be more than 110 km further than usual (Figure 3B). This observation highlights the role of advective processes on MHWs.

The link described above between the mesoscale circulation and the presence of MHWs may also explain MHWs' subsurface signal. Surface temperature anomalies can be advected southward by eddies and penetrate deeper in the water column. Eddies can also trap and advect northern water masses southward, forming an anticyclonic meander in the Polar Front, and eventually generating a temperature anomaly across the water column. MHWs could be triggered by the southward advection of water masses across the Polar Front, e.g. within mesoscale eddies or front meanders, which would essentially drive WWs distribution further southward. This study shows that indeed MHWs are associated with a lower probability of presence of WWs (Figure 4A). WWs northernmost extension (at least 80% of probability of presence) is shifted southward by around 1.4° latitude on average during MHWs in the Southern Indian Ocean. MHWs can therefore be associated with the variability of the Polar Front position, if the definition is taken of the Polar Front as the northernmost boundary of WWs. Such relation between MHWs and front shifts has already been observed in other regions (e.g. East Asian Marginal Seas, Choi et al., 2022, or the Kuroshio-Oyashio system, Du et al., 2022). The observed warming and deepening of WWs, also across all longitudes (Figure 4 B and C) is not contradictory with advective processes, as the southward shift of WWs distribution can lead to deeper and warmer WWs replacing shallower and colder WWs.

In addition to advective processes, locally enhanced mixing could contribute to extending temperature anomalies at depth, especially in highly energetic regions such as east of the Kerguelen Plateau (Dove et al., 2022). The observed warming of WWs (Figure 4C) can also be due to vertical mixing of the cold subsurface water mass with warmer surface water (Giddy et al., 2023). Giddy et al., (2023) show that a

warming trend of 0.2°C over 28 days in the WW layer was driven by a convergence of heat flux from both above and below the WW layer; since in our study we find WWs temperature anomalies of 0.33°C during MHWs (Figure 4C), diffusive processes may not be negligible.

4.2. Projected southward shift and warming of WWs in CMIP6 models

Intensity, duration, and extension of MHWs are expected to increase in the future both globally and in the Southern Indian Ocean. At the global scale, the average global number of MHW days is projected to increase by a factor of 16 even in a 1.5°C warming world (Frölicher et al., 2018). In addition, MHWs are projected to be more intense and to last longer, mostly due to ocean warming, especially in the subantarctic Indian Ocean (Azarian et al., 2023). An almost permanent state of MHW, relative to the historical period (1984-2014), is almost reached west of the Kerguelen Plateau (311.8 annual MHW days) at the end of the century using CMIP6 models under SSP2-4.5 (Azarian et al., 2023). Here we discuss the potential shift and warming of WWs under global warming on decadal timescales in both observations and CMIP6 analysis.

4.2.1. Comparing CMIP6 projections to past observations and paleoceanographic reconstructions

Our study shows a southward shift of WWs under global warming and thus of the Polar Front if this front is defined as the northernmost extension of WWs, using WWs probability of presence as an indicator (see section 3.2). The amplitude of this shift varies depending on the models but it can already be observed for a GWL 1.5°C. In a 1.5°C warming world, a maximum shift of around 4° latitude southward is found at 72°E (i.e. over the Kerguelen Plateau; compared to its preindustrial position; Figure 7).

This climate change signal may not have emerged yet in the observations. Different results have been found regarding actual trends in Polar Front shift depending on the front detection method used

(Chapman et al., 2020). There is a consensus today that there is no evidence of a southward shift of the mean ACC position from observations (Gille, 2014; Chambers et al., 2018; Pauthenet et al., 2018 ; Meredith et al., 2019). Over the past decades the Polar Front may have remained within its natural range of latitude. This is also what is observed with the MERCATOR product using the definition of the Polar Front applied in our study (i.e. northernmost boundary of WW). In particular, although an increase in MHW occurrence is observed east of the Kerguelen Plateau over the period 1993-2019, using OSTIA dataset, there is no significant increase in MHWs that are associated with a southward shift of WWs (Supplementary Material S6). In this study, we also find no significant southward shift of WWs, using MERCATOR reanalysis between 1993 and 2019 (Supplementary Materials S6). Instead, we do observe a northward shift of around 2° latitude of the Polar Front west of the Kerguelen Plateau between 47° and 65°E (Supplementary Materials S6). However, also in this area, no causal relation between Polar Front shift and occurrence of MHWs can be identified, because no significant trend in MHWs is observed using the OSTIA dataset. We thus conclude that, over the last 30 years, the position of the Polar Front and the SST may still be dominated by natural variability (Azarian et al., 2023).

However, a shift of the Polar Front, and thus of WWs, in the Southern Indian Ocean might have already occurred in a warmer world in the past (Civel-Mazens et al., 2021). During peak-Interglacials, the Polar Front was found to pass through the Fawn Trough instead of nearby Kerguelen Islands ; in our study, th is regime shift of the Polar Front is also found at the end of the century in some models and for high GWLs (e.g. 4.5°C; Figure 6D).

Such projected shift could be due to changes in air-sea interactions, advection and sea ice dynamics which all drive WWs characteristics (Gordon and Huber, 1984; Sharma and Matthew., 1985; Toole et al., 1981; Evans et al., 2018 ; Pauthenet et al., 2018). In particular, changes in freshwater fluxes, notably due to Antarctic sea ice melting and change in sea-ice transport, could be an important driver of WWs mass transformation (Abernathey et al., 2016; Haumann et al., 2016). Sea ice melting and meltwater advection in summer contributes to making WWs colder than subantarctic summer surface water (Park

et al., 1998; Anilkumar et al., 2015). If sea ice volume decreases, so might the supply of WWs and possibly their extension.

We remind that different metrics can be used to define the Polar Front (Chapman et al., 2020). Therefore, whether the Polar Front may shift in the future might vary depending on the region studied and the definition used. For instance, a water mass based definition of a front, or a surface temperature contour, might not always be well suited to follow future change of the jet position, at least regionally (Meijers et al., 2019). Jets and fronts of the Southern Indian Ocean could be controlled by different dynamical and non dynamical processes, thus generating a decorrelation between the jets and the fronts position under global warming but this would require further investigation.

4.2.2. Ecological implications of a projected asymmetrical southward shift of winter waters

In the long term, a drastic change in the WWs extension, and thus of the Polar Front, could have a significant impact on the composition and spatial distribution of the ecosystems. The changes caused by extreme events will tend to become average states depending on the GWL (WWs southward shift and warming; Figures 6 and 8), except for potential effects on WWs depth which are more uncertain (see section 3.2; Supplementary Material S4).

The asymmetry of the WWs southward shift in the CMIP6 models between the western side and the eastern side of the Kerguelen Plateau (Figure 7) indicates that eastern ecosystems may be somehow shielded by climate change. This buffering effect against climate change observed on the eastern side of the Plateau could provide a "refuge" to some species of the Kerguelen Plateau. The concept of "climate refugia" has been introduced to identify local areas undergoing limited or slower changes in climate, and are typically potential candidates for protection (Burrows et al., 2014; Brito-Morales et al., 2018). In this

27

study, the spatial differentiation of climate change impacts observed in CMIP6 models could be useful to guide conservation measures implemented in the French Southern Lands.

This contrast between the west and the east of Kerguelen Plateau also echoes the differences in vulnerability to a warming ocean observed between Crozet and Kerguelen king penguins' populations (*Aptenodytes patagonicus*, Bost et al., 2015 ; Brisson-Curadeau et al., 2022). It was found that, over the last 25 years, king penguins from Crozet were more sensitive to prey distance to the colony, associated with the fluctuations of the Polar Front position, than king penguins from Kerguelen. It was suggested that this latter population can be positively impacted by a warming ocean, through an increase in prey abundance and growth rates, as foraging areas east of Kerguelen are more stable (Bost et al., 2015; Brisson-Curadeau et al., 2022). However, these studies did not take into account that there may be a warming threshold (around 2.6°C, see section 3.2; Figure 7C) when the Polar Front might no longer be stable east of the Kerguelen Plateau. An ocean warmer than 2.6°C could then have dire consequences on the Kerguelen king penguins and on other predators that rely on WWs in the vicinity of their colonies. Note that this warming threshold is higher than the 1.5°C target of the Paris Agreement, which illustrates how committing to strong mitigation policies could significantly alleviate climate change pressure on biodiversity.

28

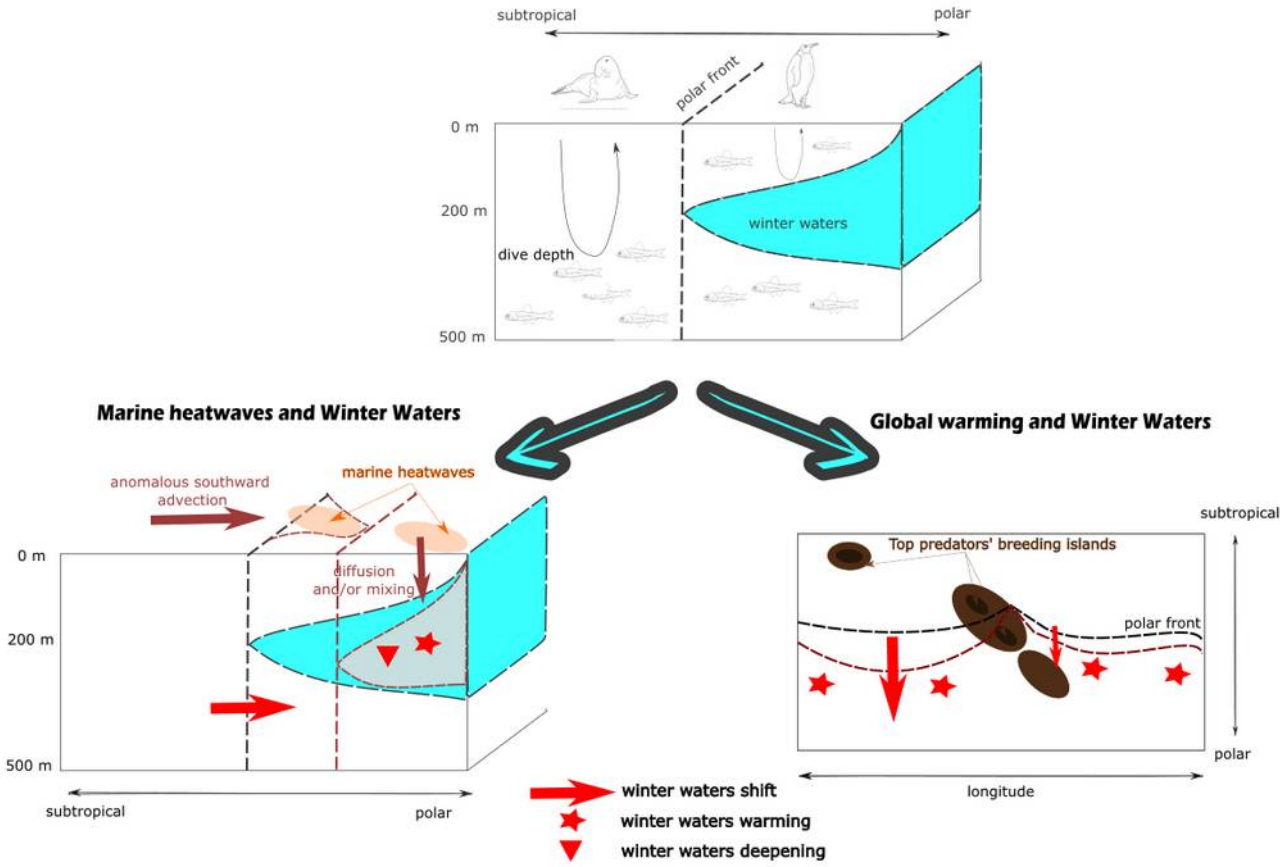

Figure 9: Summary of the impacts of marine heatwaves and long-term global warming on winter waters, whose presence and characteristics play an important ecological role, notably for Southern Indian Ocean land-based top predators.

5. Conclusion

Winter Waters (WWs) refers to a subsurface water mass, characterized by a temperature minimum between 100 m and 400 m. This water mass plays an important ecological role in the Southern Indian Ocean, often constraining the foraging areas of several predator species. In the context of climate change, the aim of this study is to shed light on the impact of a warming climate on WWs. We found that WWs presence, temperature and depth can strongly be impacted by warming at different timescales (Figure 9). In the recent decades (most recent 30 years), extreme local warming events (MHWs) are found to be related to changes in the distribution of WWs: their northernmost extension (at least 80% of

29

probability of presence) is shifted southward by around 1.4° latitude during MHWs. Under global warming, this southward shift of WWs could be increased and maintained in the long term. In particular, WWs northernmost extension is projected to shift southward by around 2.5° latitude under a 2°C warming world between 50° and 90°E using 12 CMIP6 models.

If MHWs ecological impacts can generally be limited in time and space, major extreme events such as the 1997 MHW (Bost et al., 2015) have been associated with dramatic consequences on land-based marine top predators. Impacts during such extreme events may foreshadow long-term changes for ecosystems in the future. WWs response to warming, however, is not homogeneous in our study area. CMIP6 projections suggest that the position of WWs east of the Kerguelen Plateau is relatively more stable, at least up to 2.6°C global warming. The presence of WWs nearby Kerguelen's colonies of top predators could therefore be preserved under a Paris Agreement scenario.

This study therefore points out how warming can affect ecologically significant subsurface physical features which are crucial for pelagic ecosystems. Understanding how such features might change spatially and at different timescales could be useful for policy-makers to account for climate change impacts in conservation and for mitigation strategies.

Acknowledgement

Publicly available datasets were analyzed in this study. The OSTIA, AVISO and Mercator reanalysis products were downloaded from copernicus marine service (https://marine.copernicus.eu/). The Argo data were downloaded from Argo GDAC Data Browser (https://www.usgodae.org/cgi-bin/argo_select.pl), and these data are collected and made freely available by the International Argo Program and the national programs that contribute to it (https://argo.ucsd.edu, https://www.ocean-ops.org). The Argo Program is part of the Global Ocean Observing System. The elephant seal data are collected and made freely available by the International MEOP Consortium and the national programs that contribute to it (http://www.meop.net). Both French and Australian MEOP data were used. The Australian seal tracking data are collected by the Integrated

Marine Observing System (IMOS). IMOS is a national collaborative research infrastructure, supported by the Australian Government. It is operated by a consortium of institutions as an unincorporated joint venture, with the University of Tasmania as Lead Agent. CMIP6 models outputs are publicly available here: https://esgf-node.llnl.gov/projects/cmip6/.

We acknowledge the World Climate Research Programme's Working Group on Coupled Modelling, that is responsible for CMIP. The authors also thank the IPSL modeling group for the software infrastructure, which facilitated CMIP analysis. We acknowledge funding support from the program LEFE led by CNRS-INSU, France and from the program TOSCA led by CNES, France (projects KERTREND and KERTREND-SAT). C.A. was financially supported by the French Ministry of Ecological Transition. L.B. acknowledges funding from the European Union's Horizon 2020 research and innovation program under grant agreement no. 820989 (project COMFORT). S.S. and J-B.S received funding from the European Union's Horizon 2020 research and innovation program under Grant Agreement 821001 (SO-CHIC). S.S. is also supported by a Wallenberg Academy Fellowship (WAF 2015.0186) and the Swedish Research Council (VR 2019-04400).

Appendix A : Supplementary Materials

31

References

Abernathey, R. P., Cerovecki, I., Holland, P. R., Newsom, E., Mazloff, M., and Talley, L. D. (2016). Water-mass transformation by sea-ice in the upper branch of the Southern Ocean overturning, *Nat. Geosci.*, 9, 596–601. https://doi.org/10.1038/ngeo2749

Allegue, H., Guinet, C., Patrick, S. C., Hindell, M. A., McMahon, C. R., & Réale, D. (2022). Sex, body size, and boldness shape the seasonal foraging habitat selection in southern elephant seals. *Ecology and Evolution*, 12, e8457. https://doi.org/10.1002/ece3.8457

Anilkumar, N., George, J., Chacko, R., Nuncio, N., & Sabu, P. (2015). Variability of fronts, fresh water input and chlorophyll in the Indian Ocean sector of the Southern Ocean. *New Zealand Journal of Marine and Freshwater Research*, *49*(1), 20-40. https://doi.org/10.1080/00288330.2014.924972

Argo (2000). Argo float data and metadata from Global Data Assembly Centre (Argo GDAC). SEANOE. https://doi.org/10.17882/42182

Armour, K.C., J. Marshall, J.R. Scott, A. Donohoe and E.R. Newsom (2016). Southern Ocean warming delayed by circumpolar upwelling and equatorward transport. *Nature Geoscience*, 9, 549–554.

Auger, M., Morrow, R., Kestenare, E., Sallée, J.-B., and Cowley, R. (2021). Southern Ocean in-situ temperature trends over 25 years emerge from interannual variability. *Nat Commun* 12, 514 . https://doi.org/10.1038/s41467-020-20781-1.

Azarian, C., Bopp, L., Pietri, A., Sallée, J.B. and d'Ovidio, F., (2023). Current and projected patterns of warming and marine heatwaves in the Southern Indian Ocean. Progress in Oceanography, p.103036. doi.10.1016/j.pocean.2023.103036.

Bailleul, F., Cotté, C., and Guinet, C. (2010). Mesoscale eddies as foraging area of a deep-diving predator, the southern elephant seal. *Marine Ecology Progress Series*, 408, 251-264. https://doi.org/10.3354/meps08560

659

660 Béhagle, N., Cotté, C., Lebourges-Dhaussy, A., Roudaut, G., Duhamel, G., Brehmer, P., Josse, E., and
661 Cherel, Y. (2017). Acoustic distribution of discriminated micronektonic organisms from a bi-frequency
662 processing : The case study of eastern Kerguelen oceanic waters. *Progress in Oceanography*, *156*,
663 276-289. https://doi.org/10.1016/j.pocean.2017.06.004

664 Belkin, I.M., and Gordon, A.L. (1996). Southern Ocean fronts from the Greenwich meridian. *Journal of*
665 *Geophysical Research*, 101 (2), 3675-3696

666 Biuw, M., Boehme., L., Guinet, C., Hindell, M., Costa, D., Charrassin, J.-B., Roquet, F., Bailleul, F.,
667 Meredith, M., Thorpe, S., Tremblay, Y., McDonald, B., Park, Y.-H., Rintoul, S.R., Bindoff, N., Goebel,
668 M., Crocker, D., Lovell, P., Nicholson, J., Monks, F., and Fedak, M.A. (2007). Variations in behavior
669 and condition of a Southern Ocean top predator in relation to in situ oceanographic conditions.
670 *Proc.Natl Acad. Sci*., 13 705–13. doi:10.1073/pnas.0701121104

671 Bost, C. A., Cotté, C., Bailleul, F., Cherel, Y., Charrassin, J. B., Guinet, C., Ainley, D. G., and
672 Weimerskirch, H. (2009). The importance of oceanographic fronts to marine birds and mammals of the
673 southern oceans. *Journal of Marine Systems*, *78*(3), 363-376.
674 https://doi.org/10.1016/j.jmarsys.2008.11.022

675 Bost, C. A., Cotté, C., Terray, P., Barbraud, C., Bon, C., Delord, K., Gimenez, O., Handrich, Y., Naito,
676 Y., Guinet, C., and Weimerskirch, H. (2015). Large-scale climatic anomalies affect marine predator
677 foraging behaviour and demography. *Nature Communications*, *6*(1), 8220.
678 https://doi.org/10.1038/ncomms9220

679 Brisson-Curadeau, É., Elliott, K., and Bost, C.-A. (2022). Contrasting bottom-up effects of warming
680 ocean on two king penguin populations. *Global Change Biology*, *n/a*(n/a).
681 https://doi.org/10.1111/gcb.16519

Brito-Morales, I., García Molinos, J., Schoeman, D. S., Burrows, M. T., Poloczanska, E. S., Brown, C. J., Ferrier, S., Harwood, T. D., Klein, C. J., McDonald-Madden, E., Moore, P. J., Pandolfi, J. M., Watson, J. E. M., Wenger, A. S., and Richardson, A. J. (2018). Climate Velocity Can Inform Conservation in a Warming World. *Trends in Ecology & Evolution*, *33*(6), 441-457. https://doi.org/10.1016/j.tree.2018.03.009

Burrows, M. T., Schoeman, D. S., Richardson, A. J., Molinos, J. G., Hoffmann, A., Buckley, L. B., Moore, P. J., Brown, C. J., Bruno, J. F., Duarte, C. M., Halpern, B. S., Hoegh-Guldberg, O., Kappel, C. V., Kiessling, W., O'Connor, M. I., Pandolfi, J. M., Parmesan, C., Sydeman, W. J., Ferrier, S., Williams, K.J., and Poloczanska, E. S. (2014). Geographical limits to species-range shifts are suggested by climate velocity. *Nature*, *507*(7493), 492-495. https://doi.org/10.1038/nature12976

Carter, L., McCave, I. N., and Williams, M. J. M. (2008). Circulation and water masses of the Southern Ocean: A review. In F. Florindo, & M. Siegert (Eds.), Developments in Earth & Environmental Sciences (Vol. 8, pp. 85–113). Amsterdam: Elsevier. https://doi.org/10.1016/S1571-9197(08)00004-9

Chambers, D.P. (2018). Using kinetic energy measurements from altimetry to detect shifts in the positions of fronts in the Southern Ocean. *Ocean Science*, 14, 105-116.https://doi.org/10.5194/os-14-105-2018

Chapman, C. C. (2017). New Perspectives on Frontal Variability in the Southern Ocean. J. Phys. Oceanogr., 47, 1151–1168, https://doi.org/10.1175/JPO-D-16-0222.1.

Chapman, C. C., Lea, M.-A., Meyer, A., Sallée, J.-B., and Hindell, M. (2020). Defining Southern Ocean fronts and their influence on biological and physical processes in a changing climate. *Nature Climate Change*, *10*(3), 209-219. https://doi.org/10.1038/s41558-020-0705-4

Chen, D., M. Rojas, B.H. Samset, K. Cobb, A. Diongue Niang, P. Edwards, S. Emori, S.H. Faria, E. Hawkins, P. Hope, P.Huybrechts, M. Meinshausen, S.K. Mustafa, G.-K. Plattner, and A.-M. Tréguier, 2021: Framing, Context, and Methods. In Climate Change 2021: The Physical Science Basis. Contribution of Working Group I to the Sixth Assessment Report of the Intergovernmental Panel on Climate Change [Masson-Delmotte, V., P. Zhai, A. Pirani, S.L. Connors, C. Péan, S. Berger, N. Caud, Y. Chen, L. Goldfarb, M.I. Gomis, M. Huang, K. Leitzell, E. Lonnoy, J.B.R. Matthews, T.K. Maycock, T. Waterfield, O. Yelekçi, R. Yu, and B. Zhou (eds.)]. Cambridge University Press, Cambridge, United Kingdom and New York, NY, USA, pp. 147–286, doi:10.1017/9781009157896.003

Choi, W., Bang, M., Joh, Y., Ham, Y.-G., Kang, N. and Jang, C.J. (2022). Characteristics and Mechanisms of Marine Heatwaves in the East Asian Marginal Seas: Regional and Seasonal Differences. *Remote Sens*, 14, 3522. https://doi.org/10.3390/rs14153522

Civel-Mazens, M., Crosta, X., Cortese, G., Michel, E., Mazaud, A., Ther, O., Ikehara, M., and Itaki, T. (2021). Antarctic Polar Front migrations in the Kerguelen Plateau region, Southern Ocean, over the past 360 kyrs. *Global and Planetary Change*, *202*, 103526. https://doi.org/10.1016/j.gloplacha.2021.103526

Cotté, C., d'Ovidio, F., Dragon, A.-C., Guinet, C., and Lévy, M. (2015). Flexible preference of southern elephant seals for distinct mesoscale features within the Antarctic Circumpolar Current. *Progress in Oceanography*, *131*, 46-58. https://doi.org/10.1016/j.pocean.2014.11.011

Cox, S.L., Authier, M., Orgeret, F., Weimerskirch, H., and Guinet, C. (2020). High mortality rates in a juvenile free-ranging marine predator and links to dive and forage ability. Ecol Evol., 10: 410–430. https://doi.org/10.1002/ece3.5905

Darmaraki, S., Somot, S., Sevault, F., and Nabat, P. (2019). Past Variability of Mediterranean Sea Marine Heatwaves. *Geophysical Research Letters*, *46*(16), 9813-9823. https://doi.org/10.1029/2019GL082933

Dove, L. A., Balwada, D., Thompson, A. F., and Gray, A. R. (2022). Enhanced ventilation in energetic regions of the Antarctic Circumpolar Current. *Geophysical Research Letters*, *n/a*(n/a), n/a. https://doi.org/10.1029/2021GL097574

Dragon, A.-C., Monestiez, P., Bar-Hen, A., and Guinet, C. (2010). Linking foraging behaviour to physical oceanographic structures : Southern elephant seals and mesoscale eddies east of Kerguelen Islands. *3rd GLOBEC OSM: From ecosystem function to ecosystem prediction*, *87*(1), 61-71. https://doi.org/10.1016/j.pocean.2010.09.025

Du, Y., Feng, M., Xu, Z., Yin, B., and Hobday, A.J., (2022). Summer Marine Heatwaves in the Kuroshio-Oyashio Extension Region. *Remote Sensing*, 14, (13:2980). https://doi.org/10.3390/rs141329

Elzahaby, Y., and Schaeffer, A. (2019). Observational Insight Into the Subsurface Anomalies of Marine Heatwaves. *Frontiers in Marine Science*, *6*, 745. https://doi.org/10.3389/fmars.2019.00745

Evans, D. G., Zika, J. D., Naveira Garabato, A. C., and Nurser, A. J. G. (2018). The cold transit of Southern Ocean upwelling. Geophysical Research Letters, 45, 13386–13395. https://doi.org/10.1029/2018GL079986

Eyring, V., Bony, S., Meehl, G. A., Senior, C. A., Stevens, B., Stouffer, R. J., and Taylor, K. E. (2016). Overview of the Coupled Model Intercomparison Project Phase 6 (CMIP6) experimental design and organization. *Geoscientific Model Development*, *9*(5), 1937-1958. https://doi.org/10.5194/gmd-9-1937-2016

744 Fox-Kemper, B., H.T. Hewitt, C. Xiao, G. Aðalgeirsdóttir, S.S. Drijfhout, T.L. Edwards, N.R. Golledge,
745 M. Hemer, R.E. Kopp, G. Krinner, A. Mix, D. Notz, S. Nowicki, I.S. Nurhati, L. Ruiz, J.-B. Sallée,
746 A.B.A. Slangen, and Y. Yu (2021). Ocean, Cryosphere and Sea Level Change. In Climate Change,
747 2021. The Physical Science Basis. Contribution of Working Group I to the Sixth Assessment Report of
748 the Intergovernmental Panel on Climate Change [Masson-Delmotte, V., P. Zhai, A. Pirani, S.L.
749 Connors, C. Péan, S. Berger, N. Caud, Y. Chen, L. Goldfarb, M.I. Gomis, M. Huang, K. Leitzell, E.
750 Lonnoy, J.B.R. Matthews, T.K. Maycock, T. Waterfield, O. Yelekçi, R. Yu, and B. Zhou (eds.)].
751 Cambridge University Press, Cambridge, United Kingdom and New York, NY, USA, pp. 1211–1362,
752 doi:10.1017/9781009157896.011

753 Frölicher, T. L., Fischer, E. M., and Gruber, N. (2018). Marine heatwaves under global warming.
754 *Nature*, *560*(7718), 360-364. https://doi.org/10.1038/s41586-018-0383-9

755 Giddy, I.S., Fer, I., Swart, S., and Nicholson, S-A. (2023). Vertical convergence of turbulent and
756 double-diffusive heat flux drives warming and erosion of Antarctic Winter Water in summer. Journal of
757 Physical Oceanography, 53, 1941-1958. https://doi.org/10.1175/JPO-D-22-0259.1.

758 Gille, ST. (2014). Meridional displacement of the Antarctic Circumpolar Current.Phil. Trans. R. Soc. A
759 372: 20130273. http://dx.doi.org/10.1098/rsta.2013.0273

760 Good, S., Fiedler, E., Mao, C., Martin, M. J., Maycock, A., Reid, R., Roberts-Jones, J., Searle, T.,
761 Waters, J., While, J., and Worsfold, M. (2020). The Current Configuration of the OSTIA System for
762 Operational Production of Foundation Sea Surface Temperature and Ice Concentration Analyses.
763 *Remote Sensing*, *12*(4), 720. https://doi.org/10.3390/rs12040720

764 Gordon, A. L. (1975). An Antarctic oceanographic section along 170°E. Deep Sea Res., 33, 357-377.
765 https://doi.org/10.1016/0011-7471(75)90060-1

766 Gordon, A. L., and Huber, B. A. (1984). Thermohaline stratification below the Southern Ocean sea ice.
767 *Journal of Geophysical Research: Oceans*, *89*(C1), 641-648.
768 https://doi.org/10.1029/JC089iC01p00641

769 Großelindemann, H., Ryan., S., Ummenhofer, C.C., Martin, T. and Biastoch, A. (2022). Marine
770 Heatwaves and Their Depth Structures on the Northeast U.S. Continental Shelf. *Frontiers in Climate*, 4
771 , 857937. https://doi.org/10.3389/fclim.2022.857937

772 Guinet, C., Vacquié-Garcia, J., Picard, B., Bessigneul, G., Lebras, Y. Dragon, A.C., Viviant, M.,
773 Arnould, J.P.Y., and Bailleul, F. (2014). Southern elephant seal foraging success in relation to
774 temperature and light conditions: insight into prey distribution. *Marine Ecology Progress Series*, 499,
775 pp.285-301.

776 Haumann, F. A., Gruber, N., Münnich, M., Frenger, I., and Kern, S. (2016). Sea-ice transport driving
777 Southern Ocean salinity and its recent trends. *Nature*, 537, 89–92, https://doi.org/10.1038/nature19101.

778 Herger, N., Sanderson, B. M., and Knutti, R. (2015). Improved pattern scaling approaches for the use in
779 climate impact studies. *Geophysical Research Letters*, *42*(9), 9. https://doi.org/10.1002/2015GL063569

780 Hobday, A. J., Alexander, L. V., Perkins, S. E., Smale, D. A., Straub, S. C., Oliver, E. C. J., Benthuysen,
781 J. A., Burrows, M. T., Donat, M. G., Feng, M., Holbrook, N. J., Moore, P. J., Scannell, H. A., Sen Gupta,
782 A., and Wernberg, T. (2016). A hierarchical approach to defining marine heatwaves. *Progress in*
783 *Oceanography*, *141*, 227-238. https://doi.org/10.1016/j.pocean.2015.12.014

784 Hu, S., Li, S., Zhang, Y., Guan, C., Du, Y., Feng, M., Ando, K., Wang, F., Schiller, A., and Hu, D.
785 (2021). Observed strong subsurface marine heatwaves in the tropical western Pacific Ocean.
786 *Environmental Research Letters*, *16*(10), 104024. https://doi.org/10.1088/1748-9326/ac26f2

787 Hunt, B. P. V., and Swadling, K. M. (2021). Macrozooplankton and micronekton community structure
788 and diel vertical migration in the Heard Island Region, Central Kerguelen Plateau. *Journal of Marine*
789 *Systems*, *221*, 103575. https://doi.org/10.1016/j.jmarsys.2021.103575

790 Kooyman, G. L., R. W. Davis, J. P. Croxall, and D. P. Costa. (1982). Diving depths and energy
791 requirements of king penguins. *Science* 217, 726-727.

792 Kooyman, G.L., Cherel, Y., Maho, Y.L., Croxall, J.P., Thorson, P.H., Ridoux, V. and Kooyman, C.A.
793 (1992). Diving Behavior and Energetics During Foraging Cycles in King Penguins. *Ecological*
794 *Monographs*, 62, 143-163. https://doi.org/10.2307/2937173

795 Lee, J.-Y., J. Marotzke, G. Bala, L. Cao, S. Corti, J.P. Dunne, F. Engelbrecht, E. Fischer, J.C. Fyfe, C.
796 1290 Jones, A. Maycock, J. Mutemi, O. Ndiaye, S. Panickal, and T. Zhou (2021). Future Global
797 Climate: 1291 Scenario-Based Projections and NearTerm Information. In Climate Change 2021: The
798 Physical Science 1292 Basis. Contribution of Working Group I to the Sixth Assessment Report of the
799 Intergovernmental Panel 1293 on Climate Change [Masson-Delmotte, V., P. Zhai, A. Pirani, S.L.
800 Connors, C. Péan, S. Berger, N. 1294 Caud, Y. Chen, L. Goldfarb, M.I. Gomis, M. Huang, K. Leitzell,
801 E. Lonnoy, J.B.R. Matthews, T.K. 1295 Maycock, T. Waterfield, O. Yelekçi, R. Yu, and B. Zhou
802 (eds.)]. Cambridge University Press, 1296 Cambridge, United Kingdom and New York, NY, USA, pp.
803 553–672, 1297 doi:10.1017/9781009157896.006

804 Llovel, W. and Terray, L. (2016).Observed southern upper-ocean warming over 2005–2014 and
805 associated mechanisms. *Environ. Res. Lett.* 11, 124023

806 McIntyre, T., Ansorge, I. J., Bornemann, H., Plötz, J., Tosh, C. A., and Bester, M. N. (2011). Elephant
807 seal dive behaviour is influenced by ocean temperature: implications for climate change impacts on an
808 ocean predator. *Marine Ecology Progress Series*, 441, 257–272. https://doi.org/10.3354/MEPS09383

809 McMahon, C.R., Hindell, M.A., Charrassin, J.-B., Corney, S., Guinet, C., Harcourt, R., Jonsen, I.,
810 Trebilco, R., Williams, G. and Bestley, S. (2019). Finding mesopelagic prey in a changing Southern
811 Ocean. *Sci Rep* 9, 19013. https://doi.org/10.1038/s41598-019-55152-4

812 Meijers, A.J.S., Meredith, M.P., Murphy, E.J., Chambers, D.P., Belchier, M., and Young, E.F. (2019).
813 The role of ocean dynamics in king penguin range estimation. *Nature Clim Change* **9**, 120–121.
814 https://doi.org/10.1038/s41558-018-0388-2

Meredith, M., M. Sommerkorn, S. Cassotta, C. Derksen, A. Ekaykin, A. Hollowed, G. Kofinas, A. Mackintosh, J. Melbourne-Thomas, M.M.C. Muelbert, G. Ottersen, H. Pritchard, and E.A.G. Schuur (2019). Polar Regions. In: IPCC Special Report on the Ocean and Cryosphere in a Changing Climate [H.-O. Pörtner, D.C. Roberts, V. Masson-Delmotte, P. Zhai, M. Tignor, E. Poloczanska, K. Mintenbeck, A. Alegría, M. Nicolai, A. Okem, J. Petzold, B. Rama, N.M. Weyer (eds.)]. Cambridge University Press, Cambridge, UK and New York, NY, USA, pp. 203–320. https://doi.org/10.1017/9781009157964.005.

Miyama, T., Minobe, S., and Goto, H. (2021). Marine Heatwave of Sea Surface Temperature of the Oyashio Region in Summer in 2010–2016. *Frontiers in Marine Science*, *7*, 1150. https://doi.org/10.3389/fmars.2020.576240

Morrison, A. K., S. M. Griffies, M. Winton, W. G. Anderson, and J. L. Sarmiento (2016). Mechanisms of Southern Ocean Heat Uptake and Transport in a Global Eddying Climate Model. *J. Climate*, 29, 2059–2075, https://doi.org/10.1175/JCLI-D-15-0579.1.

Mulet, S., Rio, M. H., Etienne, H., Artana, C., Cancet, M., Dibarboure, G., Feng, H., Husson, R., Picot, N., Provost, C. and Strub, P.T. (2021). The new CNES-CLS18 global mean dynamic topography. Ocean Sci. 17(3), 789–808. doi:10.5194/os-17-789-2021.

Oliver, E. C. J., Benthuysen, J. A., Darmaraki, S., Donat, M. G., Hobday, A. J., Holbrook, N. J., Schlegel, R. W., and Sen Gupta, A. (2021). Marine Heatwaves. *Annual Review of Marine Science*, *13*(1) , 313-342. https://doi.org/10.1146/annurev-marine-032720-095144

Oliver, E.C.J., Donat, M.G., Burrows, M.T., Moore, P.G., Smale, D.A., Alexander, L.V., Benthuysen, J.A., Feng, M., Sen Gupta, A., Hobday, A.J., Holbrook, N.J., Perkins-Kirkpatrick, S.E., Scannell, H.A., Straub, S.C. and Wernberg, T. (2018) Longer and more frequent marine heatwaves over the past century. Nat Commun 9, 1324 . https://doi.org/10.1038/s41467-018-03732-9.

Park, Y-H., and Gamberoni, L., (1993). Frontal Structure, Waters Masses and Circulation in the Crozet Basin. *Journal of Geophysical Research*, 98 (7), 12361-12385.

Park, Y.-H., Charriaud, E., and Fieux, M. (1998). Thermohaline structure of the Antarctic Surface Water/Winter Water in the Indian sector of the Southern Ocean. *Journal of Marine Systems*, *17*(1), 5-23. https://doi.org/10.1016/S0924-7963(98)00026-8

Park, Y.-H., Durand, I., 2019. Altimetry-derived antarctic circumpolar current fronts. SEANOE. doi:10.17882/59800

Park, Y.-H., Park, T., Kim, T.-W., Lee, S.-H., Hong, C.-S., Lee, J.-H., Rio, M.-H., Pujol, M.-I., Ballarotta, M., Durand, I. and Provost, C. (2019). Observations of the Antarctic Circumpolar Current over the Udintsev Fracture Zone, the narrowest choke point in the Southern Ocean. Journal of Geophysical Research: Oceans, 124, 4511–4528. https://doi.org/10.1029/2019JC015024

Pauthenet, E., Roquet, F., Madec, G., Guinet, C., Hindell, M., McMahon, C. R., Harcourt, R., and Nerini, D. (2018). Seasonal Meandering of the Polar Front Upstream of the Kerguelen Plateau. *Geophysical Research Letters*, *45*(18), 9774-9781. https://doi.org/10.1029/2018GL079614

Roemmich, D., Church, J., Gilson, J., Monselesan, D., Sutton, P., and Wijffels, S. (2015). Unabated planetary warming and its ocean structure since 2006. *Nature Clim Change* 5, 240–245. https://doi.org/10.1038/nclimate2513

Roquet, F., Williams, G., Hindell, M. A., Harcourt, R., McMahon, C., Guinet, C., Charrassin, J.-B., Reverdin, G., Boehme, L., Lovell, P., and Fedak, M. (2014). A Southern Indian Ocean database of hydrographic profiles obtained with instrumented elephant seals. *Scientific Data*, *1*(1), 140028. https://doi.org/10.1038/sdata.2014.28

Sabu, P., Libera, S. A., Chacko, R., Anilkumar, N., Subeesh, M. P., and Thomas, A. P. (2020). Winter water variability in the Indian Ocean sector of Southern Ocean during austral summer. *Understanding the link between atmospheric, physical and biogeochemical processes in the Indian sector of the Southern Ocean*, *178*, 104852. https://doi.org/10.1016/j.dsr2.2020.104852

Sallée, J.-B., Shuckburgh, E., Bruneau, N., Meijers, A. J. S., Bracegirdle, T. J., and Wang, Z. (2013). Assessment of Southern Ocean mixed-layer depths in CMIP5 models : Historical bias and forcing response. *Journal of Geophysical Research: Oceans*, *118*(4), 1845-1862. https://doi.org/10.1002/jgrc.20157

Sallée, J.-B. (2018). Southern Ocean Warming. *Oceanography*, *31*(2), 52-62. JSTOR.

Sharma, G.S., and Mathew, B. (1985). Hydrography and circulation off the Antarctic in the Indian Ocean region. *Proc. Indian Acad.* Sci, 94 (1), 13-27.

Siegelman, L., O'Toole, M., Flexas, M., Rivière, P.,and Klein, P., 2019. Submesoscale ocean fronts act as biological hotspot for southern elephant seal. Sci. Rep. 9, 5588.

Su, Z., Pilo, G. S., Corney, S., Holbrook, N. J., Mori, M., and Ziegler, P. (2021). Characterizing Marine Heatwaves in the Kerguelen Plateau Region. *Frontiers in Marine Science*, *7*, 1119. https://doi.org/10.3389/fmars.2020.531297

Toole, J.M. 1981. Sea ice, winter convection and temperature minimum layer in the Southern Ocean. J. Geophys. Res. 86, 8037-8047.

Treasure, A. M., Roquet, F., Ansorge, I. J., Bester, M. N., Boehme, L., Bornemann, H., Charrassin, J.-B., Chevallier, D., Costa, D. P., Fedak, M. A., Guinet, C., Hammill, M. O., Harcourt, R. G., Hindell, M. A., Kovacs, K. M., Lea, M.-A., Lovell, P., Lowther, A. D., Lydersen, C., McIntyre, T., McMahon, C.R., Muelbert, M.M.C., Nicholls, K., Picard, B., Reverdin, G., Trites, A.W., Williams, G.D., and de Bruyn, P. J. N. (2017). Marine Mammals Exploring the Oceans Pole to Pole : A Review of the MEOP Consortium. *Oceanography*, *30*(2), 132-138.

887

888

889

890

891

892

893

894

895

896

897

898

899

900

901

902

43